Dynamic charge interactions create surprising rigidity in the ER/K α-helical protein motif

Sivaraj Sivaramakrishnan*, Benjamin J. Spink*, Adelene Y. L. Sim†, Sebastian Doniach†‡, and James A. Spudich*§

Departments of *Biochemistry, †Applied Physics, and ‡Physics, Stanford University, Stanford, CA 94305

Contributed by James A. Spudich, June 30, 2008 (sent for review June 9, 2008)

Protein α-helices are ubiquitous secondary structural elements, seldom considered to be stable without tertiary contacts. However, amino acid sequences in proteins that are based on alternating repeats of four glutamic acid (E) residues and four positively charged residues, a combination of arginine (R) and lysine (K), have been shown to form stable α-helices in a few proteins, in the absence of tertiary interactions. Here, we find that this ER/K motif is more prevalent than previously reported, being represented in proteins of diverse function from archaea to humans. By using molecular dynamics (MD) simulations, we characterize a dynamic pattern of side-chain interactions that extends along the backbone of ER/K α-helices. A simplified model predicts that side-chain interactions alone contribute substantial bending rigidity (0.5 pN/nm) to ER/K α-helices. Results of small-angle x-ray scattering (SAXS) and single-molecule optical-trap analyses are consistent with the high bending rigidity predicted by our model. Thus, the ER/K α-helix is an isolated secondary structural element that can efficiently span long distances in proteins, making it a promising tool in designing synthetic proteins. We propose that the significant rigidity of the ER/K α-helix can help regulate protein function, as a force transducer between protein subdomains.

MD simulations | protein structure | single-molecule analysis | small-angle x-ray scattering

The α-helix has been found to be a ubiquitous secondary structural element in proteins since its presence was inferred by Pauling *et al.* (1). However, in naturally occurring proteins, α-helices are rarely thought of as independent protein structural elements, stable in solution in the absence of tertiary interactions (2). In folded proteins, α-helices are considered to be stabilized by exclusion of water from the hydrophobic protein core and/or by specific electrostatic interactions with neighboring secondary structures (3). Destabilization of α-helices in the absence of tertiary interactions is, thus, thought to be a consequence of competition for hydrogen bonding between the amide hydrogen in the α-helical backbone with either water oxygen in aqueous solutions or carbonyl oxygen in the backbone (4, 5).

However, there are a few known examples of α-helices that are stable in solution in the absence of tertiary interactions, including a fragment of the central region of smooth muscle caldesmon ($\approx$160 residues) (6), a segment of the tail domain of myosin X ($\approx$36 residues) (7), and the medial tail (MT) domain of myosin VI ($\approx$70 residues) (8). A common feature of these α-helices is an alternating pattern of approximately four negative (E) and approximately four positive (R/K) amino acids (6–8). Functionally, these α-helices have been suggested to bridge two different protein domains, as in caldesmon and myosin VI, and potentially extend the lever arm of the mechanoenzymes myosin VI and myosin X (6–8). How this pattern of charged residues confers stability on such α-helices, has not been clear.

Studies of the stability of isolated α-helices have almost exclusively used short ($<$20 residues) synthetic alanine-based α-helices (9–11). Polyalanine peptides form stable α-helices in solution, with α-helical content augmented by the presence of organic solvents (12). Alanine α-helices are relatively flexible structures that appear as fluctuating semibroken rods (11). Short alanine-based peptides containing an occasional single type of charged amino acid (E, R, or K) have enhanced α-helical content compared with α-helices consisting of alanine only (13, 14). The enhanced α-helical content of alanine peptides with occasional E, R, or K has been attributed to their ability to sequester water from the carbonyl oxygen and amide hydrogen groups in the α-helical backbone (4, 9). Experiments examining sparse E–K interactions in alanine α-helices suggest that E–K charge interactions do not augment α-helical content relative to alanine α-helices with only one of E, R, or K (10, 13, 15).

In contrast, the α-helical content of peptides containing only E and K (no alanine) depends on the specific distribution of E and K within the sequence (16). Specifically, the α-helical content of $(E_4K_4)_n$ is substantially higher than that of $(E_2K_2)_n$ for the same number of amino acid residues (16). This trend is reflected in the sequences of the few known naturally occurring stable α-helices of caldesmon, myosin VI, and myosin X, which follow the $(E_4K_4)_n$ pattern more closely than the $(E_2K_2)_n$ pattern (6–8). In these three proteins, it is seen that R can be substituted for K, giving alternating repeats of approximately four E residues and approximately four positively charged residues, a combination of R and K (which we denote R/K). Also, the E and R/K residues are sparsely interspersed with hydrophobic residues (A, L, I, V, and M), along with glutamine (Q) and aspartic acid (D). We refer to this general $(E_4(R/K)_4)_n$ pattern as the ER/K motif.

The dynamics of E and R/K side-chain interactions and their potential contributions to structural properties of ER/K α-helices are unknown. In this study, we use replica-exchange MD (REMD) simulations to examine the equilibrium conformations of ER/K α-helices. We use information derived from the MD simulations to construct a simplified theoretical model for the bending rigidity of ER/K α-helices. The stability and rigidity of ER/K α-helices are independently examined by a combination of SAXS and single-molecule optical-trap analyses of a sample ER/K α-helix, namely the MT of myosin VI.

Results and Discussion

ER/K α-Helix Is Recurrent in Nature. The number of both known and hypothetical or predicted protein sequences in the database with the ER/K motif is revealed by a BLAST search in the PubMed database of nonredundant protein sequences including all species. To ensure a nonbiased evaluation of search hits, $(E_4K_4)_2$ and $(E_4R_4)_2$ were used as search templates, and the list of sequences that scored better than any species of myosin X or myosin VI was examined to assess the relative number of proteins that contain the ER/K motif. Because tail fragments in myosin VI and myosin X are known to be isolated α-helices in solution, we propose that our search criteria provide a conser-

Author contributions: S.S. and J.A.S. designed research; S.S., B.J.S., and A.Y.L.S. performed research; S.D. contributed new reagents/analytic tools; S.S., A.Y.L.S., and J.A.S. analyzed data; and S.S., B.J.S., A.Y.L.S., S.D., and J.A.S. wrote the paper.

The authors declare no conflict of interest.

§To whom correspondence should be addressed. E-mail: jspudich@stanford.edu.

This article contains supporting information online at www.pnas.org/cgi/content/full/0806256105/DCSupplemental.

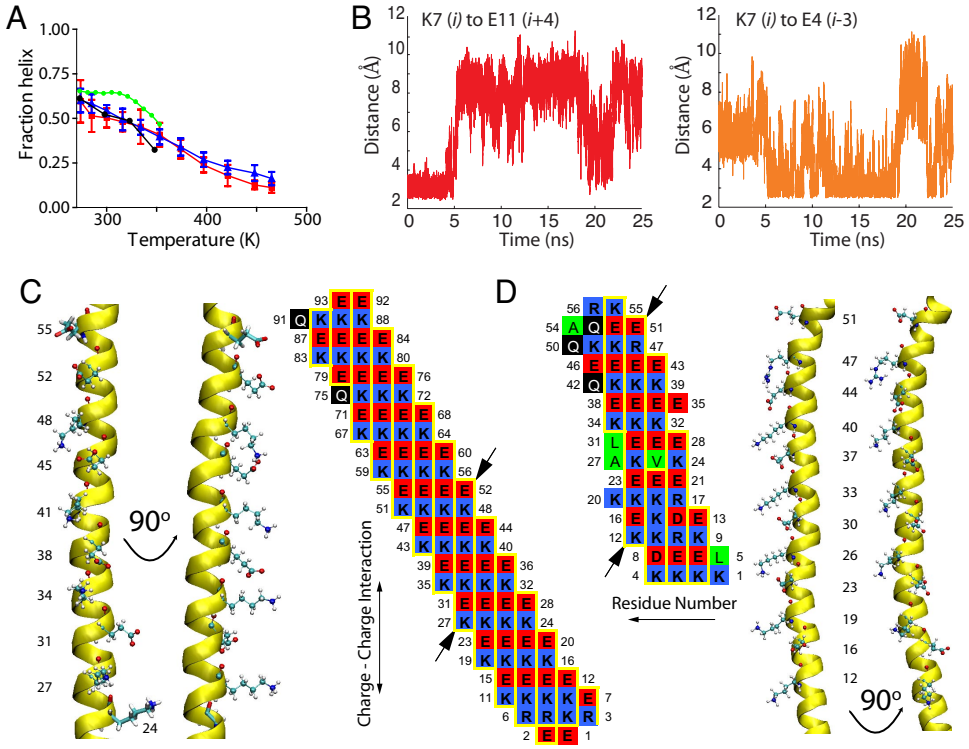

Fig. 1. Charge interactions along the ER/K α-helix backbone. (*A*) Fraction helix as a function of temperature from experiment (CD melt) and computation (REMD). Blue, REMD data starting with α-helical conformation; red, REMD data starting with random initial conformation; black, CD-melt data from Lyu *et al.* (16); green, CD melt data for the MT ER/K α-helix in myosin VI. CD data were converted to fraction helix as per Rohl and Baldwin (28). (*B*) With reference to an $(E_4K_4)_2$ helix (E1 to K16), sample variation of distance (Å) between N_ζ atom of K7 (*i*) and center of mass of O_ε atoms of E4 ($i-3$) (*Right*) and E11 ($i+4$) (*Left*) with time (ns) during MD simulations (*Left*). (*C*) (*Left*) Snapshot of two orthogonal views of a section of the ER/K α-helix (residues 24–55) in mannosyltransferase from the MD simulation, showing side-chain interactions and residue numbers. For reference, the backbone carbonyl oxygens corresponding to the illustrated side chains are also shown. (*Right*) The charge interaction map (see *SI Methods*) shown to the right illustrates the pattern of E↔R/K interactions along the vertical axis (see yellow boxed groups of residues in columns). Arrows show boundaries of the segment of the α-helix displayed in *Left*. (*D*) Snapshot of two orthogonal views of a section of the ER/K helix (residues 12–51) in upf2 regulator of nonsense transcripts homolog (*Right*), with its charge interaction map (*Left*).

vative estimate of similar α-helices in other protein structures. We find the ER/K motif is present in at least 123 known distinct proteins in 137 organisms ranging from archaea to humans, with at least 20 distinct proteins in mammals [e.g., supporting information (SI) Table S1]. As mentioned above, the ER/K motifs in the three proteins that are known to form stable α-helices in solution are sparsely interspersed with residues A, L, I, V, M, Q, and D. The relative content of residues E, R, and K in these helices is 70% in caldesmon, 78% in myosin X, and 79% in myosin VI. When we analyzed the results of the BLAST search for continuous ER/K regions matching the search criteria, with the boundaries of this region determined by the presence of amino acids not listed above, we found that the mean content of E, R, and K in helices obtained from the search is 80%. By using this approach, the ER/K motif is >30 residues in at least 40 distinct proteins with the longest continuous ER/K region being 346 residues for a Kelch motif family protein in *Trichonomis vaginalis G3*.

MD Simulations Reveal Dynamic Charge Interactions in ER/K α-Helices. To understand the effects of E and R/K side-chain interactions on the stability and function of ER/K α-helices, we performed REMD simulations on the sample sequence $(E_4K_4)_2$ in explicit solvent. We selected $(E_4K_4)_2$ as a suitable candidate because it allows the side chains to sample multiple interactions (*i* to $i \pm n$ where $n = 1$–7) and seek out the most energetically favorable ones. Also, $(E_4K_4)_2$ is known have high α-helical content in solution with known temperature, pH, and salt-concentration dependence, as measured by circular dichroism (CD) (16). These experimental measurements provide a quantitative benchmark of our REMD simulations. Last, the $(E_4K_4)_2$ sequence is well represented in the protein mannosyltransferase (*Saccharomyces cerevisiae*), which contains four continuous perfect repeats of $(E_4K_4)_2$. In the absence of known crystal structures of ER/K α-helices, we performed REMD simulations starting with the $(E_4K_4)_2$ peptides in both random (no secondary structure) and fully α-helical conformations (see *Methods*). Convergence of simulation was assessed by insignificant differences in fraction helix (see *SI Methods*) at all simulated temperatures (Fig. 1*A* and Fig. S1). The convergence of two different initial conditions to a unique solution is essential to obtain equilibrium conformations for both the peptide backbone and side-chain interactions, especially because the objective of these MD simulations is to study side-chain interactions.

The thermal melt curves obtained from REMD (Fig. 1*A*) are very similar to experimental data obtained for $(E_4K_4)_2$ by using CD (16). CD data for the MT segment of myosin VI are shown in Fig. S2 with the fraction helix displayed in Fig. 1*A*. The fraction helix for the myosin VI MT with ≈70 residues is higher than that for $(E_4K_4)_2$ with 16 residues, as expected due to the increased length of the peptide chain (11).

We used REMD simulations to equilibrium sample a large range of protein conformations by using finite computing power (17). However, due to periodic exchange between different replicas, REMD does not provide trajectories of side-chain interactions in real time. To obtain this information, we randomly selected $(E_4K_4)_2$ replicas that were completely folded from random initial configuration and equilibrated them in

BIOPHYSICS

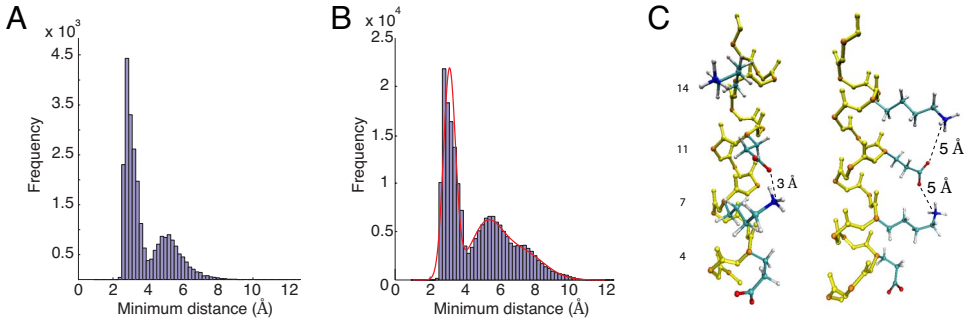

Fig. 2. Side-chain interaction distances in the $(E_4K_4)_2$ α-helix. (*A*) Histogram of minimum distance, at every time step of the MD simulation, between K7-N_ζ and the centers of mass of O_ε in neighboring E residues. For the entire simulation time, K7-N_ζ is closest to one of E3, E4, E10, and E11. (*B*) Histogram of minimum distances, at every time step of the MD simulation, between N_ζ of each K residue and centers of mass of O_ε in all neighboring E residues and vice versa. The red line shows a maximum likelihood fit to the sum of three Gaussians, which yields the relative time spent under the 3, 5, and 8-Å peaks along with their standard deviations. (*C*) Snapshot of the $(E_4K_4)_2$ α-helix showing sample side-chain conformations during 3-Å (*Left*) and 5-Å (*Right*) separations between $N_\zeta$and O_ε.

explicit solvent for 25 ns at 274 K. These simulations were continued for an additional 25 ns with trajectories of all protein atoms monitored over this time period. The N_ζ atom of residue K7 (i) oscillates between the center of mass of the two O_ε atoms of E4 ($i - 3$) and E11 ($i + 4$) (Fig. 1*B*). The center of mass of the two O_ε atoms of E10 (i), alternately, oscillates between the N_ζ atom of residue K6 ($i - 4$) and K13 ($i + 3$) (data not shown). This preference for ($i - 3$)/($i + 4$) interactions at K(i) residues and ($i - 4$)/($i + 3$) interactions at E (i) residues is seen for all of the center eight residues (K5-E12) of the $(E_4K_4)_2$ helix. The preference for these interactions is reflected in the histograms of the frequency of all distances for $i - 3/4$ and $i + 3/4$ interactions, at each of the eight residues K5–E12. These histograms reveal clear 3-Å peaks for the specific interactions listed above (Fig. S3). Residues in the first turn of the helix (E1–E4) do not have $i - 3$ and $i - 4$ interactions, whereas residues in the last turn of the helix (K13–K16) do not have $i + 3$ and $i + 4$ interactions.

Closer examination of the instantaneous structures of the folded $(E_4K_4)_2$ α-helices show that the particular pattern of interactions for E and K residues arises from a combination of the following: permissible dihedral angles between the peptide backbone and the C_α–C_β side chain of the E and K residues; and the right-handed structure of the α-helix causing residues to rise left to right from the N to the C terminus of the peptide backbone of the α-helix (Fig. 1 *C* and *D*). For example, K27, E31, K34, E38, K41, E45, K48, and E52 form a network of interactions that spans nearly 4 nm along one face of the α-helix (Fig. 1*C*). This alternating pattern of + 4 then + 3 closely approximates 3.6 residues per turn of an α-helix. Therefore, the ER/K motif allows for continuous series of interactions along the same face of the α-helical backbone. We use this alternating pattern of + 4 then + 3 to draw a map of preferred interactions along the α-helical backbone, both for the extended $(E_4K_4)_n$ helix and for ER/K α-helices in general (Fig. 1*C* and Fig. S4). A striking feature in such maps is several continuous series of interactions in all ER/K α-helices (Fig. 1 *C* and *D*; boxes in yellow). In the $(E_4K_4)_n$ α-helix, eight residues form a chain of oscillating interactions, whereas in upf-2 regulator of nonsense transcripts (Table S1) we see a maximum of 12 residues (Fig. 1*D*, arrows).

The oscillation of E and K side chains between their $i - 3/4$ and $i + 3/4$ neighbors implies that at every time step of the MD simulation, the minimum distance between each N_ζ of K and the centers of mass of O_ε of all its E neighbors (and vice versa) is the dominant contributor to the interaction between E and K side chains. Fig. 2*A* shows the histogram of these minimum distances collected >25 ns for residue K7, and Fig. 2*B* shows the combined histogram of these minimum distances for residues K7 through K12. The preference for ($i - 3$)/($i + 4$) interactions at K(i) residues and ($i - 4$)/($i + 3$) interactions at E(i) residues, described above, holds true in this combined histogram, in that for 90% of the simulation time the closest pairing residue for K or E follows this preferred pattern. The histogram can be best characterized by a maximum-likelihood fit to the sum of three Gaussian distributions (*SI Methods*) with centers located at 3, 5, and 8 Å. The relative times spent in the three modes of interaction, in turn, are given by the areas under the individual Gaussian distributions to be 45%, 37%, and 18%, respectively. Detailed examination of interatomic distances reveals that the interaction centered at 3 Å corresponds to hydrogen bonding between the H_ζ of K and O_ε of E (Fig. 2*C* and Fig. S5). For the interaction centered at 5 Å, the E and K side chains are located approximately equidistant from their $i - 3/4$ and $i + 3/4$ neighbors (Fig. 2*C*). For these conformations, we find that the O_ε atom of E is located 3–6 Å from H atoms in the K side chain, suggesting a combination of direct interaction through Coulomb forces between opposite charges and indirect interactions through solvent-separated salt-bridge contacts (Fig. S5). The third peak centered at 8 Å has contributions from the following: the continuous series of alternating E and K interactions located seven residues apart implies that residues K8 and E9 do not have $i - 3$ and $i + 3$ neighbors, respectively (Fig. S3); and due to oscillations of side chains between their $i - 3/4$ and $i + 3/4$ pairs, each side chain spends a small fraction of its time (<10%) without an interacting partner.

Side-Chain Interactions Significantly Influence The Stability and Rigidity of ER/K α-Helices. The stability of isolated α-helices in the presence of polar solvents such as water is limited by disruption of hydrogen bonds in the α-helical backbone (4, 5). Previous comparisons of MD simulations of alanine-based α-helices with SAXS measurements suggest that these helices undergo continuous transient breaks in the α-helical backbone that reduce the end-to-end distance of the α-helix (11). Our MD simulations show that there are multiple E and R/K side-chains interactions for each turn of the ER/K α-helix, which prevent transient breaks in backbone hydrogen bonds from unraveling the α-helix. Additionally, the ER/K α-helix partially excludes water molecules from the backbone (Fig. 3*A*), approximately to the same extent as the alanine-based F_s peptide (simulation data not shown). This partial water exclusion is potentially a combination of space occupied by the long E and R/K side chains and the hydrophobic methylene groups in them. Therefore, outer charges in the E and R/K side chains that interact favorably, along with inner hydrophobic groups that exclude water molecules, offer a unique combination to stabilize the backbone conformation of ER/K α-helices in the aqueous cellular environment.

There are two potential sources of bending rigidity of isolated

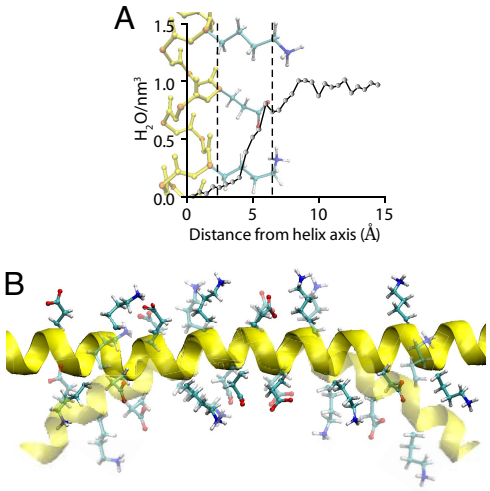

Fig. 3. Lateral bending and stability of ER/K α-helix. (*A*) Water density as a function of distance from the α-helix axis for the $(E_4K_4)_2$ α-helix. The vertical dotted line at 2.2 Å shows the average location of C_α atoms, whereas the vertical dotted line at 6 Å shows the average location of N_ζ/O_ε atoms of the K/E side chains. Note the exclusion of water from the α-helical backbone resulting from the presence of side chains. (*B*) Exaggerated schematic representation showing bending of the ER/K α-helix in mannosyltransferase. The α-helix backbone is shown in ribbon representation (yellow), along with selected E and K side chains. To illustrate the effect of bending on side-chain interaction distances, the bent α-helix is shown as a transparent structure. The α-helix bending approximately the neutral axis results in an increase in E↔K distances on the convex side (top face), with a corresponding decrease in E↔K distances on the concave side (bottom face).

ER/K α-helices, the α-helical backbone and side-chain interactions. Previous computational analyses of alanine α-helices that ignore transient breaks in the α-helical backbone report a bending stiffness of ≈1 pN/nm (scaled for a 10-nm long α-helix) (18, 19). However, in the presence of polar solvent, with partial water exclusion, the contribution of the α-helical backbone to the bending stiffness is unclear. With regard to side-chain contribution to bending stiffness, the backbone carbonyl oxygen, amide hydrogen, and C_α atoms are of 2.2 Å from the helix axis, whereas N_ζ and O_ε of the K and E side chains, respectively, are located on average at 6 Å from the axis of the ER/K α-helix. Thus, bending forces on the ER/K α-helix will first be "sensed" and, therefore, resisted by side-chain interactions before they propagate to the backbone (Fig. 3*B*). In this regard, the E and R/K side-chain interactions resemble a continuous narrow tube of radius 6 Å that reinforces the bending rigidity of ER/K α-helices. To examine the contribution of E and R/K side-chain interactions to the bending rigidity, we use a simplified model for the bending of the ER/K α-helix as a cantilever beam with side-chain interactions representing the elastic elements that resist bending (Fig. S6). Our model is valid only for external mechanical forces applied over time scales that are significantly greater (10 μs) than the dynamic time scale for side-chain interactions shown here (100 ns). Fig. 3*B* shows an exaggerated schematic of the bending of the α-helix with the resulting deformations along the α-helical backbone.

To estimate the stiffness of individual side-chain interactions, we interpret the two Gaussian distributions centered at 3 and 5 Å as representing two favored potential wells. The width of these three Gaussian distributions can be used to estimate the harmonic spring constants of 3,200 and 440 pN/nm, respectively, for these potential wells. Whereas the hydrogen bonding interaction at 3 Å is approximately 10-fold stronger than the 5-Å one, the softer 5-Å interaction has an approximately 3-fold greater reach due to larger standard deviation (0.3 vs. 0.9 Å). For side-chain-interaction distances corresponding to the 5-Å potential well, each E (i) interacts simultaneously with K ($i - 4$) and K ($i + 3$). However, for the 3-Å potential well, each E (i) interacts with only one of K ($i - 4$) and K ($i + 3$). Thus, the 5-Å potential well, in addition to its longer reach, provides a continuous sheet of interactions without breaks along the α-helical backbone. Therefore, we model the side-chain interactions as a continuous narrow tube with stiffness corresponding to the 5-Å potential well. We thus estimate a stiffness of 0.5 pN/nm entirely from side-chain interactions (Fig. S6 and *SI Methods*). Our model suggests that the ER/K α-helix can act as a relatively stiff structural element in mechanoenzymes such as myosin VI and X, based on side-chain interactions alone.

Single-Molecule Analyses and SAXS Are Consistent with High Rigidity of ER/K α-Helices. We studied the contribution of the MT of myosin VI (MT ER/K α-helix) to its effective lever arm stroke under load applied by a dual beam optical trap (see *Methods*) (20). The myosin VI lever arm strokes through ≈180° parallel to the F-actin filament (21), resulting in a lateral bending force transmitted through the MT ER/K α-helix (Fig. 4*A*). A measure of the stroke size of two myosin VI constructs, one that extends to the beginning and another to the end of the MT ER/K α-helix, enabled us to measure the deflection of the MT ER/K α-helix under lateral bending load.

To characterize the stroke of myosin VI, it is essential to understand the structural elements involved in the myosin VI lever arm. We have previously described the tail domain of myosin VI as being composed of three segments, a globular proximal tail (PT), a central region containing the MT ER/K α-helix, and a terminal globular segment containing the distal tail (DT) and cargo binding domain (8). We had previously shown by using SAXS analysis that the PT alone is an ≈3-nm globular structure, whereas the SAXS envelope for the MT-DT (120 residues) is suggestive of a single α-helix (MT) coupled with a folded domain (DT).

Here, we use SAXS analysis to get insight into the contribution of the PT to the myosin VI lever arm, along with a SAXS envelope for the MT ER/K α-helix alone. To understand the contribution of the PT to the myosin VI lever arm, we obtained a SAXS envelope structure for a segment of the myosin VI molecule starting with the second IQ motif (with bound calmodulin) to the end of the PT (Fig. 4*B Upper*). Our structure for this complex comes from a fusion of the IQ-calmodulin structure-based on previously modeled myosin VI structures (22) and Rosetta prediction of the PT (see *Methods*). The IQ and PT were fused at Pro-835 and the backbone dihedral angles at the IQ–PT junction were adjusted manually to fit the structure optimally into the SAXS envelope. The modeled structure was used to predict a 15-nm stroke size of the myosin VI lever arm to the beginning of the MT ER/K α-helix (Fig. 4*A*). This prediction is verified by a 15 ± 3-nm stroke size measured in an optical trap (Fig. 4*C Upper*).

The SAXS envelope of the MT ER/K α-helix reveals an ≈10-nm long envelope that matches the predicted length of a single isolated α-helix containing ≈70 residues comprising the MT (Fig. 4*B Lower*). Interestingly, the SAXS envelope has two distinct bends whose locations along the α-helix correspond to two highly conserved hydrophobic patches along the length of the MT (Fig. 4*B Lower*). These SAXS results would be most consistent with these hydrophobic patches being relatively rigid kinks rather than flexible nodes. To understand the role of hydrophobic patches on stability of the α-helix, we performed MD simulations of different segments of the MT folded into complete α-helices and then simulated at 400 K (Fig. S7). We found that all segments of the MT remain complete α-helices, whereas the peptide $(E_2K_2)_4$ unfolds to a random coil (Fig. S7), suggesting that these hydrophobic patches in the MT do not unravel the ER/K α-helix. However, the simulations do show that regions that contain these hydrophobic residues undergo tran-

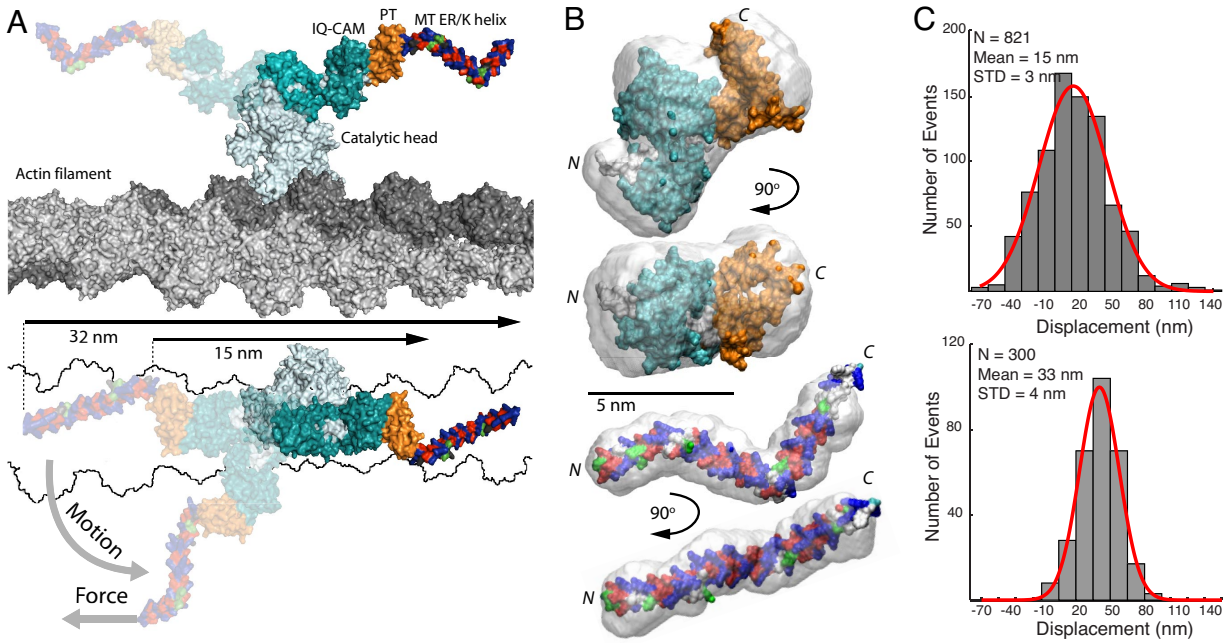

Fig. 4. Experimental verification of stability and bending rigidity of the MT ER/K α-helix in myosin VI. (*A*) Schematic of the lateral bending of the MT ER/K α-helix during the 180° swing of the myosin VI lever arm. (*Upper*) The poststroke state is indicated with the prestroke state shown as a transparent structure (side view along the actin filament). (*Lower*) The poststroke state is indicated with the prestroke state and lever arm in transition shown as transparent structures (top view along the actin filament). Distances shown in the schematic representation are derived from the known myosin VI crystal structure with modeled IQ-CAM (22) and predicted structures of the PT and MT. Although the angle between the PT and MT is unknown, the orientation shown in the schematic representation is consistent with the SAXS structures of PT-MT and PT-MT-DT published previously (8), and aligns the MT parallel to the F-actin filament to allow dimerization of the cargo binding domains, resulting in ≈36-nm processive stepping of myosin VI. (*B*) Two orthogonal views of the predicted structure of a fragment of myosin VI including the IQ motif and PT with bound calmodulin docked into its SAXS envelope. The PT is predicted to contribute only ≈1.5 nm to the lever arm of myosin VI (*Upper*). Orthogonal views of the predicted structure of the MT ER/K α-helix in myosin VI docked into its SAXS envelope. The end–end distance of the SAXS envelope (10 nm) is consistent with the ER/K motif forming an isolated, stable α-helix in solution. N and C termini are marked (*Lower*). (*C*) Histogram of bead displacement in response to binding of myosin VI to an actin filament, followed by the myosin VI power stroke. Mean displacement is a measure of the stroke size of the myosin VI lever arm without (*Upper*) and with (*Lower*) the MT ER/K α-helix.

sient unfolding and refolding more frequently than for completely charged ER/K repeats. The functional significance of this observation remains to be elucidated.

The maximal load applied in the optical trap is the stiffness of the optical trap multiplied by the stroke size (displacement of the bead). Our theoretical model predicts that side-chain interactions contribute significant stiffness to ER/K α-helices. We performed optical trapping measurements at a trap stiffness of ≈0.005 pN/nm, which should result in small deflections (<1 nm) of ER/K α-helices with a stiffness of ≈0.5 pN/nm estimated from our model (Fig. S6). We found that the stroke size of a myosin VI construct that extends to the end of the MT ER/K α-helix is 33 ± 4 nm, which is the same as the predicted stroke size of 33 nm measured from the modeled structure of the same myosin VI construct. It should be emphasized that the angle between the PT and MT ER/K α-helix is unknown. However, the orientation shown in the schematic illustration is consistent with the SAXS structures of PT-MT and PT-MT-DT published previously (8) and aligns the MT ER/K α-helix parallel to the F-actin filament to allow dimerization of the cargo binding domains and the ≈36-nm processive stepping of myosin VI (23).

In summary, we show here that the ER/K α-helix forms a relatively rigid and stable isolated secondary structural element in proteins. The ER/K α-helix is much more prevalent in protein sequences than previously reported. We find a unique oscillating interaction of charged side chains distributed along the α-helical backbone. This dynamic interaction of side chains can tolerate significant change in interaction distances that result from lateral bending of the α-helix, compared with locked interactions resulting from salt-bridge formation. We propose a model of the ER/K α-helix as a cantilever beam, which despite its many simplifications is sufficient to account for the high stiffness of the ER/K α-helix observed in both SAXS and single-molecule optical-trapping experiments. The ER/K α-helix in myosin VI, myosin X, and caldesmon acts as a bridge between protein subdomains. Specifically, in myosin VI a load applied at the end of the cargo binding domain must be transmitted through the ER/K α-helix to the head, where it is known to alter the kinetics of nucleotide binding and release (24). The rigidity of the MT ER/K α-helix is likely to impact the force transduced to the myosin VI catalytic head and, therefore, mechanosignaling of myosin VI. Last but not least, the ability of the ER/K α-helix to efficiently span large distances as an isolated protein structural element makes it a promising tool for use in designing synthetic proteins.

Methods

MD Simulations. REMD of the E_4K_4 peptide (CH_3CO-EEEEKKKKEEEEKKKK-$NHCH_3$) were performed with GROMACS (25, 26) by using the AMBER2003 force field (27). Two simulations, one starting with the peptide in complete α-helix form and the other starting with the peptide as a random coil, were performed for 80 and 42 ns, respectively, for each replica. Trajectories of side-chain interactions were determined from 50 ns simulations of individual replicas at 274 K. Details of simulation parameters and data analysis are described in *SI Methods*.

Biophysical Characterization of Segments of Myosin VI. IQ-PT (814–918 *Homo sapiens*) bound to human calmodulin in an equimolar ratio along with myosin VI MT (916–981 *H. sapiens*) were purified by using standard protein purification techniques (*SI Methods*). SAXS measurements, data analysis, and reconstructions were carried out as described in Spink *et al.* (8) (see *SI Methods* and

Fig. S8 for specific details). CD, multiangle laser light scattering (MALLS), and dynamic light scattering (DLS) measurements were carried out as described in Spink *et al.* (8) (see *SI Methods* for details).

Single-Molecule Optical-Trap Assays. Optical trapping was performed by using myosin VI molecules extending to the beginning (1–918 *Sus scrofa*) and end (1–981 *S. scrofa*) of the MT (see *SI Methods* for details). Optical trapping was performed as described in Bryant *et al.* (21).

ACKNOWLEDGMENTS. We thank M. A. Hartman (Stanford University) for technical help with protein purification and manuscript review; S. Seifert and D. S. Pavlichin for help with SAXS data collection; J. Lipfert for help with SAXS reconstructions and manuscript review; J. Liao, A. Dunn, Z. Bryant, V. S. Pande, M. Levitt, and R. L. Baldwin for critical discussions and manuscript review; and R. Sowdhamini for discussions and use of the National Center for Biological Sciences computing cluster in Bangalore, India, for preliminary simulations. Use of the Advanced Photon Source was supported by the Office of Science and Office of Basic Energy Sciences U.S. Department of Energy under Contract DE-AC02-06CH11357. The Bio-X^2 computing cluster is supported by National Science Foundation Award CNS-0619926. This work was supported by an American Cancer Society postdoctoral fellowship (to S.S.), the Agency for Science, Technology, and Research, Singapore (A.Y.L.S.), and National Institutes of Health Grants T32 GM008294 (to B.J.S.), PO1 GM066275 (to S.D.), and GM33289 (to J.A.S.).

1. Pauling L, Corey RB, Branson HR (1951) The structure of proteins; two hydrogen-bonded helical configurations of the polypeptide chain. *Proc Natl Acad Sci USA* 37:205–211.
2. Dill K, Ozkan S, Shell M, Weikl T (2008) The Protein Folding Problem. *Annu Rev Biophys* 37:289–316.
3. Daggett V, Fersht A (2003) The present view of the mechanism of protein folding. *Nat Rev Mol Cell Biol* 4:497–502.
4. Vila JA, Ripoll DR, Scheraga HA (2000) Physical reasons for the unusual alpha-helix stabilization afforded by charged or neutral polar residues in alanine-rich peptides. *Proc Natl Acad Sci USA* 97:13075–13079.
5. Cammers-Goodwin A, *et al.* (1996) Mechanism of Stabilization of Helical Conformations of Polypeptides by Water Containing Trifluoroethanol. *J Am Chem Soc* 118:3082–3090.
6. Wang CL, *et al.* (1991) A long helix from the central region of smooth muscle caldesmon. *J Biol Chem* 266:13958–13963.
7. Knight PJ, *et al.* (2005) The predicted coiled-coil domain of myosin 10 forms a novel elongated domain that lengthens the head. *J Biol Chem* 280:34702–34708.
8. Spink B, Sivaramakrishnan S, Lipfert J, Doniach S, Spudich J (2008) Long single alpha helical domains bridge the gap between structure and function of myosin VI. *Nat Struct Biol* 15:591–597.
9. Garcia AE, Sanbonmatsu KY (2002) Alpha-helical stabilization by side chain shielding of backbone hydrogen bonds. *Proc Natl Acad Sci USA* 99:2782–2787.
10. Ghosh T, Garde S, Garcia AE (2003) Role of backbone hydration and salt-bridge formation in stability of alpha-helix in solution. *Biophys J* 85:3187–3193.
11. Zagrovic B, Jayachandran G, Millett IS, Doniach S, Pande VS (2005) How large is an alpha-helix? Studies of the radii of gyration of helical peptides by small-angle X-ray scattering and molecular dynamics. *J Mol Biol* 353:232–241.
12. Scholtz JM, Baldwin RL (1992) The mechanism of alpha-helix formation by peptides. *Annu Rev Biophys Biomol Struct* 21:95–118.
13. Marqusee S, Baldwin RL (1987) Helix stabilization by Glu-.Lys+ salt bridges in short peptides of de novo design. *Proc Natl Acad Sci USA* 84:8898–8902.
14. Marqusee S, Robbins VH, Baldwin RL (1989) Unusually stable helix formation in short alanine-based peptides. *Proc Natl Acad Sci USA* 86:5286–5290.
15. Huyghues-Despointes BM, Scholtz JM, Baldwin RL (1993) Helical peptides with three pairs of Asp-Arg and Glu-Arg residues in different orientations and spacings. *Protein Sci* 2:80–85.
16. Lyu PC, Gans PJ, Kallenbach NR (1992) Energetic contribution of solvent-exposed ion pairs to alpha-helix structure. *J Mol Biol* 223:343–350.
17. Sugita Y, Okamoto Y (1999) Replica-exchange molecular dynamics method for protein folding. *Chem Phys Lett* 314:141–151.
18. Adamovic I, Mijailovich SM, Karplus M (2008) The elastic properties of the structurally characterized myosin II S2 subdomain: A molecular dynamics and normal mode analysis. *Biophys J* 94:3779–3789.
19. Choe S, Sun SX (2005) The elasticity of alpha-helices. *J Chem Phys* 122:244912.
20. Spudich JA, Rice S, Rock R, Purcell T, Warrick H (2008) *Optical Traps to Study Properties of Molecular Motors* (Cold Spring Harbor Laboratory Press, New York).
21. Bryant Z, Altman D, Spudich JA (2007) The power stroke of myosin VI and the basis of reverse directionality. *Proc Natl Acad Sci USA* 104:772–777.
22. Menetrey J, Llinas P, Mukherjea M, Sweeney HL, Houdusse A (2007) The structural basis for the large powerstroke of myosin VI. *Cell* 131:300–308.
23. Rock RS, *et al.* (2001) Myosin VI is a processive motor with a large step size. *Proc Natl Acad Sci USA* 98:13655–13659.
24. Altman D, Sweeney HL, Spudich JA (2004) The mechanism of myosin VI translocation and its load-induced anchoring. *Cell* 116:737–749.
25. Berendsen HJC, Vanderspoel D, Vandrunen R (1995) Gromacs - a message-passing parallel molecular-dynamics implementation. *Comput Phys Commun* 91:43–56.
26. Lindahl E, Hess B, Vanderspoel D (2001) GROMACS 3.0: A package for molecular simulation and trajectory analysis. *J Mol Model* 7:306–317.
27. Wang JM, Cieplak P, Kollman PA (2000) How well does a restrained electrostatic potential (RESP) model perform in calculating conformational energies of organic and biological molecules? *J Comput Chem* 21:1049–1074.
28. Rohl CA, Baldwin RL (1997) Comparison of NH exchange and circular dichroism as techniques for measuring the parameters of the helix-coil transition in peptides. *Biochemistry* 36:8435–8442.